Supporting Information:

A New Route for De-carboxylation of Lactones over Zn/ZSM-5: Elucidation of Structure and Molecular Interactions

*L. Ye, Q. Song, B.T.W. Lo, J. Zheng, D. Kong, C.A. Murray, C.C. Tang and S.C.E. Tsang**

Materials and Methods:

1.1 H-ZSM-5 pretreatment

H-ZSM-5 (Al:Si=1:19.25) was supplied from Sinopec, China. The elemental analysis of the solid samples was performed using inductively coupled plasma-atomic emission spectroscopy(P-4010/ICP-AES). The sample was calcined in air at 480 ℃ for 2 h with a ramp rate of 1 ℃ min^{-1} before use. In addition, the BET surface area of H-ZSM-5 is 330 m^2 g^{-1}.

1.2 H-ZSM-5 sample modification

Modified H-ZSM-5 with different metal ions were prepared by aqueous ion-exchange of H-ZSM-5 with La^{3+}, K^{+}, Ni^{2+}, Ce^{4+}, Sn^{4+}, Ga^{3+}, Zn^{2+} nitrate or chloride solutions. The ion-exchange was carried at ambient temperature by mixing 1.0 g H-ZSM-5 with 30 mL aqueous solution which contains an equivalent of one metal ion per H-ZSM-5 unit cell for 5 h. Then, the samples were rinsed five times with deionized water and dried at 70 °C overnight. All the samples were calcined in air at 550 °C for 5 h before catalytic testing. The Zn content was determined to be 0.91% by ICP-AES. In addition, the BET surface area of Zn/ZSM-5 is 334 m^2 g^{-1} (no apparent change in surface area as compared to the unmodified H-ZSM-5).

2 Catalytic testing

The GVL conversion was initially carried over H-ZSM-5 and modified H-ZSM-5 catalysts in a continuous flow reactor (Figure S1(a)) under industrial conditions in SRIFT, SINOPEC, China. The reaction was conducted in a fixed bed (800 mm × 13 mm) at 450 ℃ and 1.0 MPa nitrogen pressure. Before reaction, 5.0 g of catalyst (pelletized and crashed into small particles (through 20 - 40 mesh)) was loaded in the fixed bed, which was pre-treated in N_2 at 500 ℃ for 2 h at 50 mL min^{-1}. A 40 wt% aqueous GVL solution was introduced into the reactor by a HPLC pump (Series II, Scientific System Inc, USA). The liquid flow rate was 5.0 mL h^{-1}. The feedstock was preheated to 350 ℃ before entering the catalyst bed. For a comparative study, pure GVL liquid over H-ZSM-5 catalyst was also tested under the same conditions. The results showed that a rapid drop in catalytic performance.

The typical liquid product distribution using GVL-water feedstock are displayed in Figure S1(b). Typical aromatic products were benzene (B), toluene (T), xylene (X). Alkyl substituted benzene (e.g. 1-methyl-3-ethyl benzene and 1-methyl-2-ethyl benzene, n-propyl benzene), indane and alkyl substituted naphthalene were present at small quantity. Some low boiling hydrocarbons (before 5 min) were also pre-dissolved in liquid phase.

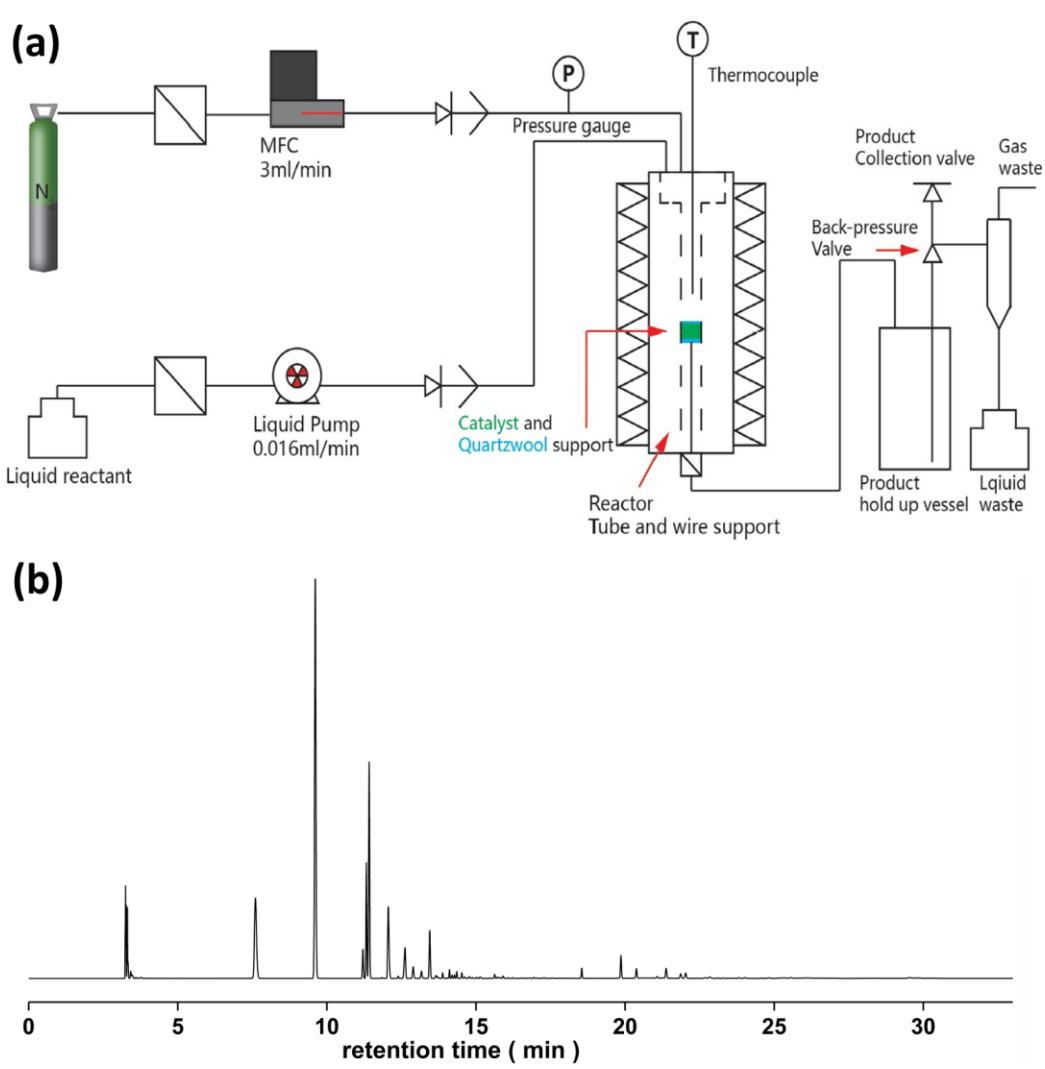

Fig. S1. (a) Typical setup of the continuous flow reactor. (b) Typical liquid product distribution in the organic layer after the catalysis of gamma-valerolactone (GVL): C_3 - C_6 hydrocarbon (3.4 - 3.5 min), benzene (7.6 min), toluene (9.6 min), xylene (11.3 min), tri- or tetramethyl benzene (12.6 - 15.0 min), naphthalene and its derivatives (over 18.0 min) by GC-MS.

The total carbon count in liquid was 89.7% (assuming 1 mole of CO_2 is produced per mole of GVL, and the CO_2 was excluded in carbon balance calculation). The gas sample was collected into a gas bag and was analyzed by GC (Agilent 6820, HP-Al/S column, 50 m × 0.53 mm × 15 um). All the gas amounts were calculated by standard curve which was calibrated by standard gas. The total carbon count in gas was 7.2%. The carbon in coke was 2.4% by TG analysis.
The composition of a set of gaseous products is listed below:

Composition	mol %
Methane	3
Ethane	3
Ethylene	1
Propane	8
Propylene	4
Isobutene	6
n-butane	7
1-butene	25
trans-2-butene	19
Isobutene	3
cis-2-butene	18
Isopentane	1

A similar continuous flow micro-reactor (Figure S1(a)) was also built at the University of Oxford, UK. 5.0 g of powder catalyst was typically loaded into a tubular quartz reactor tube (H.E.L FlowCAT) with the catalyst bed held in place by two plugs of quartz wool, and the reactor was put inside a vertical furnace. The reactor was controlled at 10 bar by a back pressure regulator. The reaction temperature was kept at 450 °C. The desired reaction temperature and pressure were achieved under flowing N_2 gas with a flow rate 50 ml min^{-1}. The aqueous solution of GVL (40 wt%) was prepared and fed to the packed tubular reactor using a HPLC pump with WHSV 1.0 h^{-1}. The liquid products and gas effluent were collected for quantitative analysis by a separator at ambient temperature and analyzed by GC or GC-MS (Agilent Technologies 5977A MSD/7890B GC system, HP-INNOWAX column 30 m × 0.25 mm, ShinCarbon column ST 80/100 2 m × 0.53 mm). The yield was calculated based on mole % of GVL converted to a specific product. The carbon mass balance was derived from all moles of carbon containing products collected as compared to the input mole of carbon from GVL with taking CO_2 into account. Almost identical catalytic performance was confirmed at the Oxford Laboratory. For the recycle reaction performed at Oxford, the WHSV and temperature were tuned to 2.0 h^{-1} and 400 °C to increase the rate of carbon deposition during the accelerated deactivation period. Before the next cycle, the deactivated catalyst was calcined in air at 600 °C for 1 h.

Aqueous solution of 40 wt% GVL was chosen as the starting substrate and was fed into pre-heated zone (350^{o}C) before the catalyst bed. It is because GVL can be obtained in 20-40 wt% aqueous solution by hydrolyzing cellulose or lignocellulose to produce levulinic acid, followed by catalytic

hydrogenation of the product in water. Purifying soluble GVL from aqueous solution is an energy intensive step as water has a very high heat capacity than other solvents and thus needing more energy input. Therefore, using GVL/water feedstock without purification to non-polar compounds such like aromatics (immiscible with water) will be an energy saving and environmental friendly process.

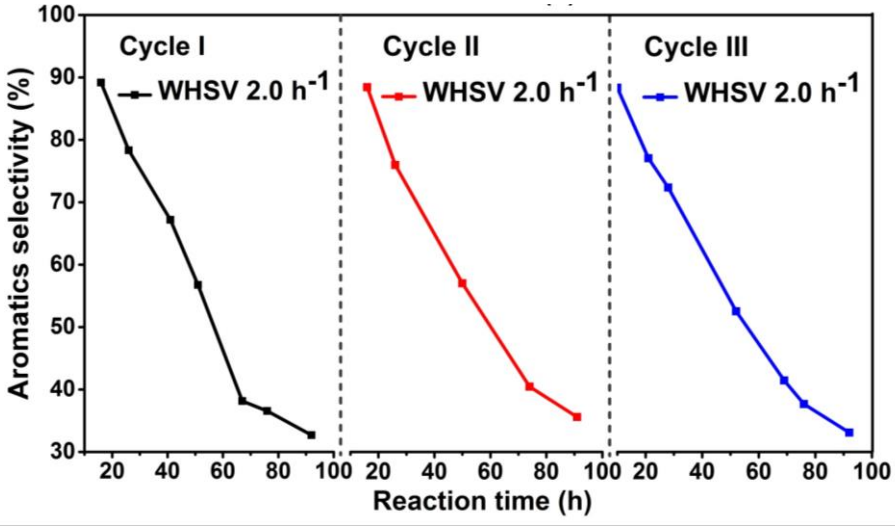

Fig. S2. Cyclic catalytic performance of Zn/ZSM-5 with WHSV 2 h^{-1} at 400 °C.

The evaluation of the Zn/ZSM-5 catalyst under accelerated deactivation conditions, using higher WHSV of 2.0 h^{-1} at 400 °C at Oxford indicated that the aromatics selectivity decreased gradually from 89.2% to 33% after 90 h in the first cycle. After switching the nitrogen carrier to air and calcined the sample at 600 °C for 1 h, the activity of the Zn/ZSM-5 was totally resumed in Cycle II and similarly to Cycle III.

3 Synchrotron XRD and Rietveld refinement

High resolution SXRD data were collected on Beamline I11, Diamond Light Source, UK. Detailed description of the beamline can be found elsewhere[1]. The energy of the incident X-ray beam was set at 15 keV. The wavelength and the 2θ-zero point correction were refined using a diffraction pattern obtained from a high quality silicon powder (SRM640c). At room temperature, the fine zeolite powder was loaded in a 0.7 mm borosilicate glass capillary. High resolution SXRD data were obtained from the samples using the multi-analyser crystal (MAC) detectors. The patterns were collected in the 2θ range 0-150° with 0.001° data step. Each pattern was collected for an hour for good statistics. In total, there were more than 4000 *hkl* reflections measured, of which at least 300 independent *hkl* reflections were observed. In a crystallographic point of view, the number of structural variables should not exceed the number of *hkl* reflections in a refinement. In the Rietveld refinements performed in this work, the number of structural parameters has not exceeded 160.

Using the TOPAS software, the diffraction patterns were analyzed by the Rietveld methods. The starting coordinates were based on the H-ZSM-5 model by Heo et al. for structural refinement[2]. The Thompson-Cox-Hastings pseudo-Voigt peak function [3] was applied to described the diffraction peaks. The scale factor and lattice parameters were allowed to refine for all the diffraction patterns. The refined structural parameters for pattern were the fractional coordinates (x, y, z) and isotropic displacement factors (B_{eq}) for all atoms, and the site occupancy factors (SOF) for all Zn species and GVL molecules, translation and rotation axes for the rigid body Z-matrices describing the octahedral Zn species and the adsorbed GVL molecules within the ZSM-5 framework. The quality of the Rietveld refinements of SXRD data has been assured with a low goodness-of-fit (gof) factor, a low weighted profile factor (R_{wp}) and a well fitted pattern with acceptable isotropic displacement factors (B_{eq}) within experimental errors. The crystallographic data and refinement details are summarized in Tables S1-5 in SI section 3.

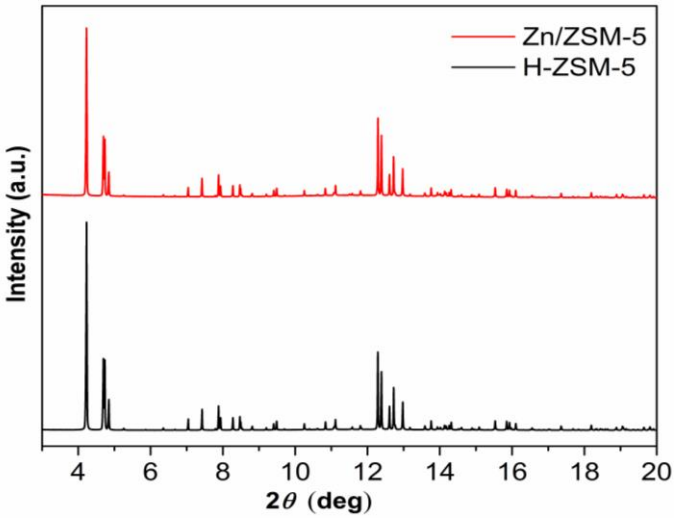

Fig. S3. Comparison of the SXRD patterns between Zn/ZSM-5 (red) and H-ZSM-5 (black) at room temperature range from 3 - 20°.

3.1 Refinement Procedure:

The SXRD data of Zn/ZSM-5 was analysed by Pawley and Rietveld refinements of Zn/ZSM-5 with and without Zn. They are presented in Section S3.2. Full CIF files in table format and detailed profile fit plots with enlarged ranges are given.

According to our refinement procedure, Zn atoms were added into H-ZSM-5 one by one (Zn1, Zn2, Zn3…). The R-factors (R_{wp} / R_p / R_{exp} / χ^2) were used to gauge the quality of refinement. With the progressive increase in the number of Zn atoms, the R-factors were found decreasing, which indicates the use of Zn is approaching to the real structure (Table S1). It was until the third Zn, the R-factor was almost remained unchanged. However, the pseudo 'third' Zn appeared at an unreasonable position, i.e. inside the framework of H-ZSM-5 with extremely low site occupancy 0.0082(9). Thus, we excluded the third Zn. As a result, two Zn positions were used to the fittings of all the SXRD data accordingly.

Table S1. R-factors of Zn/ZSM-5 sample by Pawley and Rietveld method.

Samples	Pawley R_{wp} / R_p / R_{exp} / χ^2	Rietveld R_{wp} / R_p / R_{exp} / χ^2
H-ZSM-5· 0Zn	6.553/4.975/3.384/1.936	8.649/6.806/3.529/2.451
H-ZSM-5· 1Zn	6.553/4.975/3.384/1.936	8.197/6.377/3.529/2.322
H-ZSM-5· 2Zn	6.553/4.975/3.384/1.936	7.896/6.087/3.525/2.240
H-ZSM-5· 3Zn	6.553/4.975/3.384/1.936	7.887/6.094/3.529/2.235

The number (before Zn) in the sample name column means the number of Zn positions that have been used. The R-factors from Pawley fit were optimized without any constraints of the structural models in contrast to the Rietveld-fit, hence accounting for their lower values.

Table S2. Crystallographic data and details of Zn/ZSM-5 samples before and after GVL adsorption.

Samples	Zn/ZSM-5	GVL adsorbed Zn/ZSM-5	Regenerated Zn/ZSM-5
Crystal system	Orthorhombic	Orthorhombic	Orthorhombic
Space group	*Pnma*	*Pnma*	*Pnma*
Chemical formula	$H_{4.74}Al_{4.74}Si_{91.26}O_{192} \cdot 1$ Zn	$H_{4.74}Al_{4.74}Si_{91.26}O_{192} \cdot 1$ Zn (GVL)	$H_{4.74}Al_{4.74}Si_{91.26}O_{192} \cdot 1$ Zn
2 θ range refinement (^{o})	3 – 55	3 – 55	3 – 55
Detector	Multi-analyser crystals crystals	Multi-analyser crystals	Multi-analyser crystals
Number of parameters	148	144	159
Number of hkls	4186	4186	4170
Refinement methods	Rietveld	Rietveld	Rietveld
a (Å)	20.12885(3)	20.12918(4)	20.12332(4)
b (Å)	19.95555(3)	19.95527(4)	19.93119(4)
c (Å)	13.43143(3)	13.43088(3)	13.40047(3)
V (Å^3)	5395.172(27)	5394.959(36)	5374.683(48)
R_{wp} / R_p / R_{exp} (%)	7.896/6.086/3.529	8.550/6.698/4.021	9.583/7.361/2.713
Wavelength (Å)	0.825900(2)	0.825868(2)	0.825903(2)
2θ Zero point (°)	-0.004944(2)	-0.004293(2)	-0.005480(2)
Gof χ^2	2.237	2.127	3.532

3.2 The SXRD and Rietveld refinement of Zn/ZSM-5 at room temperature.

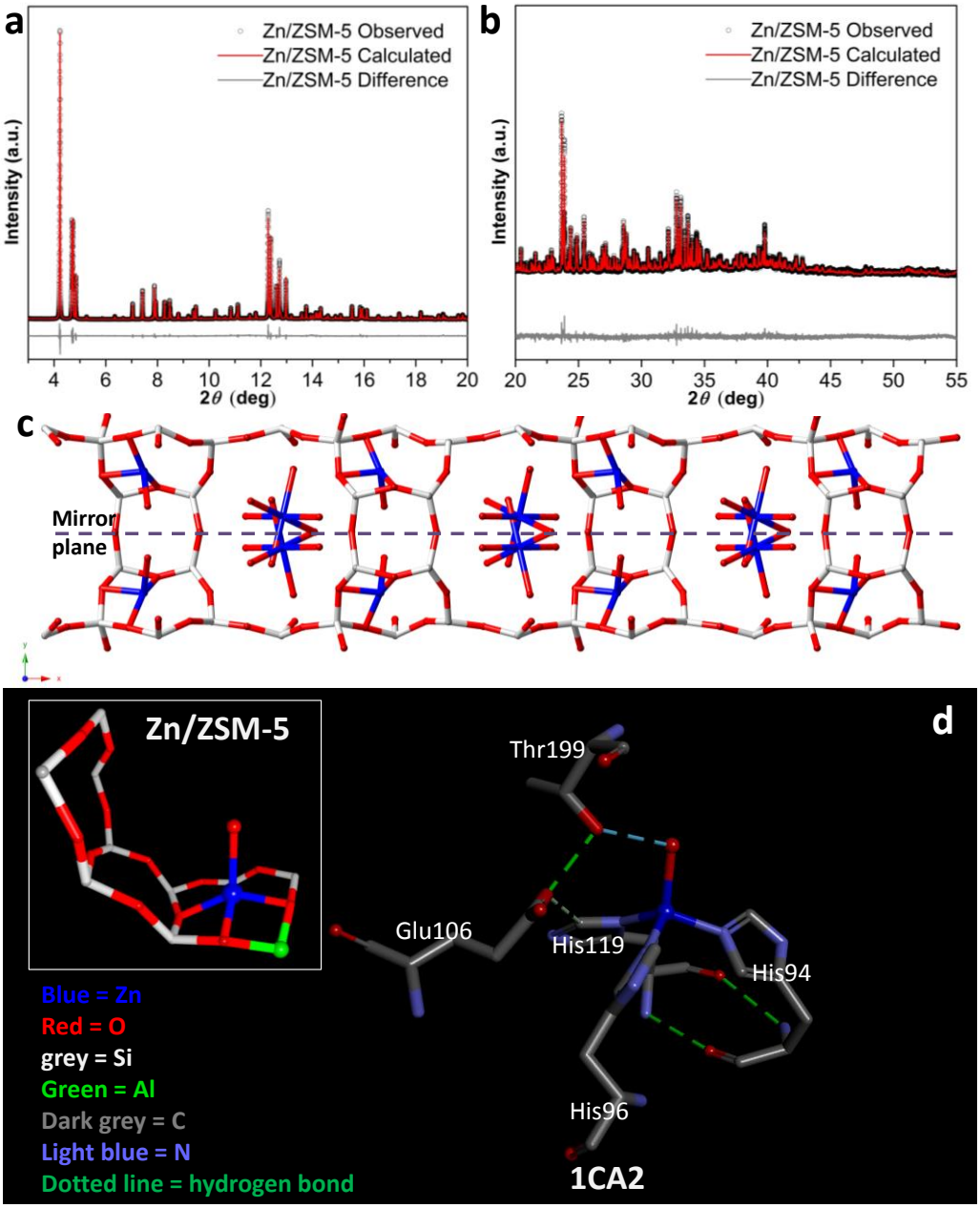

Fig. S4. SXRD with the Rietveld refinement and the structure of Zn/ZSM-5 at room temperature. Comparison of the experiment data (black circle) and Rietveld refinement (red line) and the difference between them (grey line) for SXRD patterns of Zn/ZSM-5 at room temperature at a 2θ range of (a) 3 - 20° and (b) 20 - 55°. (c) The refined structure of Zn/ZSM-5 (viewed from z-axis). (d) Comparison of the geometry of the Zn active site in Zn/ZSM-5 and the natural enzyme T199A CAII (PDB: 1CA2)[4]. The stick-ball model is used, with red = O, grey = Si, and blue = Zn. The symmetric Zn species between the mirror plane are illustrated (grey dotted line).

Table S3. Atomic parameters from the Rietveld refinement of Zn/ZSM-5 at room temperature.

Species	Atom	*x*	*y*	*Z*	SOF	B_{eq} (Å^2)	Wyckoff
Zeolite framework	O1	0.37534(41)	0.05998(44)	0.75634(51)	1	3.162(33)	8d
	O2	0.30852(41)	0.06392(34)	0.92286(51)	1	3.162(33)	8d
	O3	0.19936(37)	0.06248(34)	0.02036(36)	1	3.162(33)	8d
	O4	0.09660(32)	0.05942(42)	0.91524(55)	1	3.162(33)	8d
	O5	0.11409(39)	0.04755(49)	0.73157(53)	1	3.162(33)	8d
	O6	0.24562(38)	0.04613(50)	0.75403(52)	1	3.162(33)	8d
	O7	0.37129(43)	0.84717(42)	0.76213(58)	1	3.162(33)	8d
	O8	0.30718(44)	0.84727(30)	0.92797(51)	1	3.162(33)	8d
	O9	0.19298(41)	0.84592(25)	0.02861(41)	1	3.162(33)	8d
	O10	0.08869(36)	0.84006(36)	0.92130(63)	1	3.162(33)	8d
	O11	0.11853(44)	0.84122(40)	0.73403(56)	1	3.162(33)	8d
	O12	0.24445(46)	0.84050(43)	0.76023(62)	1	3.162(33)	8d
	O13	0.31172(38)	0.95176(40)	0.82323(37)	1	3.162(33)	8d
	O14	0.07629(30)	0.95320(44)	0.82288(44)	1	3.162(33)	8d
	O15	0.41756(37)	0.12185(39)	0.59787(57)	1	3.162(33)	8d
	O16	0.40306(40)	0.99571(40)	0.59239(60)	1	3.162(33)	8d
	O17	0.40119(40)	0.86793(37)	0.57318(62)	1	3.162(33)	8d
	O18	0.18991(48)	0.12994(34)	0.61613(47)	1	3.162(33)	8d
	O19	0.20092(49)	0.00283(36)	0.59363(51)	1	3.162(33)	8d
	O20	0.19764(48)	0.87069(35)	0.58273(48)	1	3.162(33)	8d
	O21	0.99607(40)	0.04867(50)	0.79614(47)	1	3.162(33)	8d
	O22	0.99711(44)	0.85163(43)	0.79477(49)	1	3.162(33)	8d
	O23	0.42002(54)	0.7500	0.64499(66)	1	3.162(33)	4c
	O24	0.19445(68)	0.7500	0.65775(59)	1	3.162(33)	4c
	O25	0.28290(48)	0.7500	0.05561(70)	1	3.162(33)	4c
	O26	0.10353(54)	0.7500	0.05963(80)	1	3.162(33)	4c

	Si1	0.42180(20)	0.05861(27)	0.66258(31)	1	1.309(15)	8d
	Si2	0.30903(28)	0.02941(17)	0.81279(32)	1	1.309(15)	8d
	Si3	0.27978(17)	0.06190(22)	0.03485(29)	1	1.309(15)	8d
	Si4	0.12177(18)	0.06289(23)	0.02602(31)	1	1.309(15)	8d
	Si5	0.06889(21)	0.02935(20)	0.81760(34)	1	1.309(15)	8d
	Si6	0.18615(22)	0.05581(23)	0.67469(28)	1	1.309(15)	8d
	Si7	0.42467(22)	0.82990(20)	0.67103(34)	1	1.309(15)	8d
	Si8	0.30720(26)	0.86994(20)	0.81691(29)	1	1.309(15)	8d
	Si9	0.27366(20)	0.82692(19)	0.02870(32)	1	1.309(15)	8d
	Si10	0.11940(21)	0.82681(21)	0.03012(36)	1	1.309(15)	8d
	Si11	0.07193(22)	0.87211(23)	0.81566(33)	1	1.309(15)	8d
	Si12	0.18877(27)	0.82612(17)	0.68528(32)	1	1.309(15)	8d
Zn-1	Translate	0.9290(8)	0.7173(11)	0.1885(10)			
	Zn1	0.9290	0.7173	0.1885	0.104(2)	8.1(12)	4c
	$Zn1O_W1$	0.9060	0.6164	0.1529	0.104(2)	12.1(19)	4c
	$Zn1O_W2$	0.8513	0.7182	0.2951	0.104(2)	12.1(19)	4c
	$Zn1O_W3$	0.9963	0.6840	0.2994	0.104(2)	12.1(19)	4c
	$Zn1O_W4$	1.0066	0.7164	0.0819	0.104(2)	12.1(19)	4c
	$Zn1O_W5$	0.8616	0.7506	0.0777	0.104(2)	12.1(19)	4c
	$Zn1O_W6$	0.9519	0.8181	0.2242	0.104(2)	12.1(19)	4c
Zn-2	Zn2	0.7774(11)	0.1209(12)	0.8225(17)	0.071(3)	16.3(21)	8d
OZn2	$Zn2O_W1$	0.7858(12)	0.3052(17)	0.6895(21)	0.071(3)	24.4 (31)	8d

All the T-sites (T=Al, Si) of ZSM-5 were refined using the same B_{eq} parameter.

All the O-sites of ZSM-5 were refined using the same B_{eq} parameter.

The values for the O-sites of Zn species were refined using the same SOF and 1.5 times of the B_{eq} for the coordinated Zn-sites.

3.3 The SXRD and Rietveld refinement of GVL adsorbed on fresh Zn/ZSM-5 at room temperature.

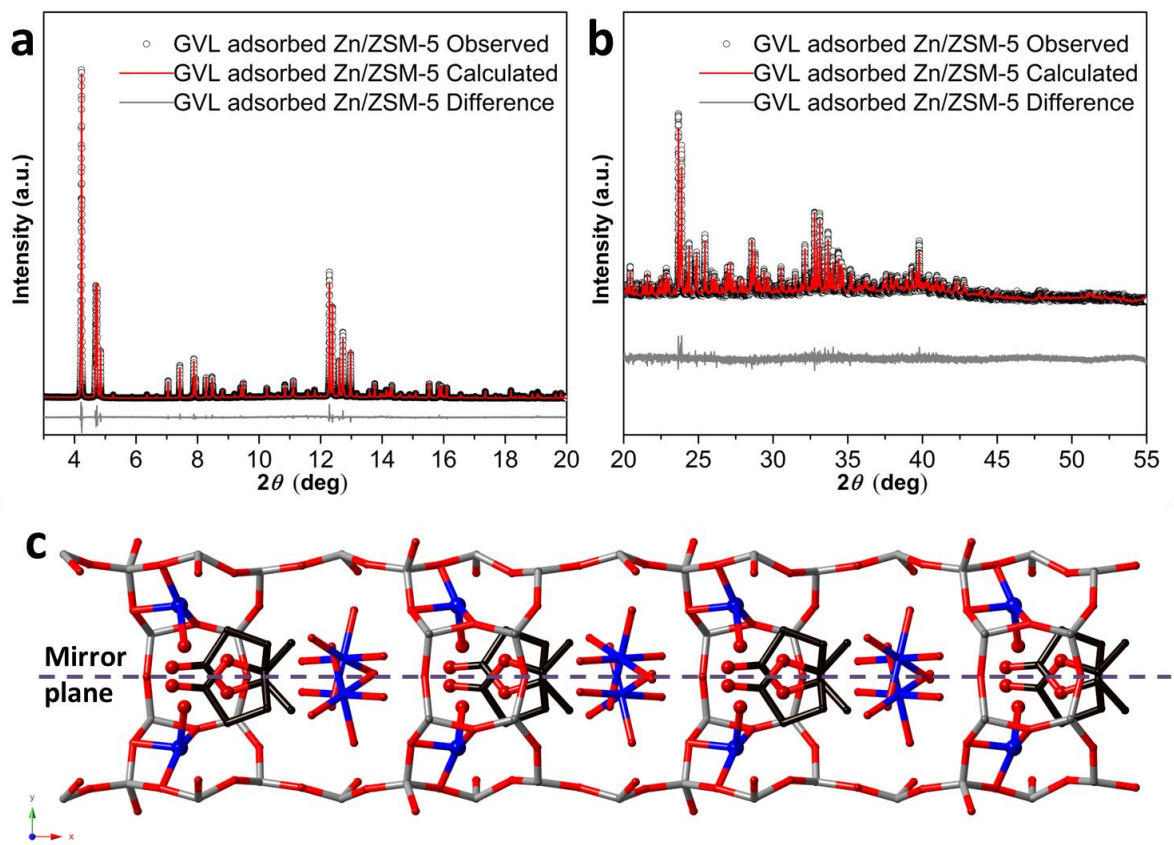

Fig. S5. SXRD with the Rietveld refinement and the structure of GVL adsorbed on fresh Zn/ZSM-5 at room temperature. (a) Comparison of the experiment data (black circle) and Rietveld refinement (red line) and the difference between them (grey line) for SXRD patterns after GVL adsorbed Zn/ZSM-5 at room temperature at a 2θ range of (a) 3 - 20° and (b) 20 - 55°. (c) The refined structure of adsorbed GVL on Zn/ZSM-5 (viewed from z-axis). The stick-ball model is used, with red = O, grey = Si, and blue = Zn, black = C. The symmetric Zn species and GVL between the mirror plane are illustrated (grey dotted line).

Table S4. Atomic parameters from the Rietveld refinement of fresh Zn/ZSM-5 after GVL adsorption at room temperature.

Species	Atom	*x*	*y*	*Z*	SOF	B_{eq} (Å^2)	Wyckoff
Zeolite framework	O1	0.37545(52)	0.06228(55)	0.75285(66)	1	3.386(45)	8d
	O2	0.31077(51)	0.06193(46)	0.92307(65)	1	3.386(45)	8d
	O3	0.19708(50)	0.06391(42)	0.01745(47)	1	3.386(45)	8d
	O4	0.09757(41)	0.05899(54)	0.91213(72)	1	3.386(45)	8d
	O5	0.11427(52)	0.04634(62)	0.72846(69)	1	3.386(45)	8d
	O6	0.24477(50)	0.04731(65)	0.76072(68)	1	3.386(45)	8d
	O7	0.37307(55)	0.84379(51)	0.76741(77)	1	3.386(45)	8d
	O8	0.30589(58)	0.84518(40)	0.92808(66)	1	3.386(45)	8d
	O9	0.19357(54)	0.84558(33)	0.03289(50)	1	3.386(45)	8d
	O10	0.08705(45)	0.84098(47)	0.92560(83)	1	3.386(45)	8d
	O11	0.11792(58)	0.84164(51)	0.73857(78)	1	3.386(45)	8d
	O12	0.24573(60)	0.84525(58)	0.75269(87)	1	3.386(45)	8d
	O13	0.31637(44)	0.95215(53)	0.82724(48)	1	3.386(45)	8d
	O14	0.07779(38)	0.95457(58)	0.82530(58)	1	3.386(45)	8d
	O15	0.42053(49)	0.12168(50)	0.59886(74)	1	3.386(45)	8d
	O16	0.40289(52)	0.99448(49)	0.59311(77)	1	3.386(45)	8d
	O17	0.39890(52)	0.86515(46)	0.57219(80)	1	3.386(45)	8d
	O18	0.19392(64)	0.12999(44)	0.61793(59)	1	3.386(45)	8d
	O19	0.20179(62)	0.00620(45)	0.58924(67)	1	3.386(45)	8d
	O20	0.19889(61)	0.87642(44)	0.58943(61)	1	3.386(45)	8d
	O21	0.99695(54)	0.04874(67)	0.79316(60)	1	3.386(45)	8d
	O22	0.99560(57)	0.85380(55)	0.79533(64)	1	3.386(45)	8d
	O23	0.42216(70)	0.7500	0.64223(86)	1	3.386(45)	4c
	O24	0.19485(84)	0.7500	0.67462(74)	1	3.386(45)	4c
	O25	0.28189(62)	0.7500	0.05260(89)	1	3.386(45)	4c

	O26	0.10111(69)	0.7500	0.05730(103)	1	3.386(45)	4c
	Si1	0.42194(27)	0.05936(34)	0.66072(39)	1	1.381(20)	8d
	Si2	0.31068(34)	0.02893(23)	0.81262(40)	1	1.381(20)	8d
	Si3	0.27850(24)	0.06274(29)	0.03456(38)	1	1.381(20)	8d
	Si4	0.12072(24)	0.06207(31)	0.02490(41)	1	1.381(20)	8d
	Si5	0.06878(28)	0.02844(26)	0.81897(43)	1	1.381(20)	8d
	Si6	0.18588(29)	0.05569(29)	0.67558(37)	1	1.381(20)	8d
	Si7	0.42441(29)	0.83025(26)	0.67130(44)	1	1.381(20)	8d
	Si8	0.30645(34)	0.87016(26)	0.81598(38)	1	1.381(20)	8d
	Si9	0.27429(27)	0.82739(25)	0.03041(43)	1	1.381(20)	8d
	Si10	0.11981(28)	0.82704(27)	0.03055(46)	1	1.381(20)	8d
	Si11	0.07251(28)	0.87199(31)	0.81472(43)	1	1.381(20)	8d
	Si12	0.18890(36)	0.82670(23)	0.68360(42)	1	1.381(20)	8d
Zn-1	Translate	0.9290(8)	0.7173(11)	0.1885(10)			
	Zn1	0.9290	0.7173	0.1885	0.104(2)	4.9(10)	4c
	$Zn1O_W1$	0.9080	0.6270	0.1570	0.104(2)	7.3(15)	4c
	$Zn1O_W2$	0.8590	0.7190	0.2840	0.104(2)	7.3(15)	4c
	$Zn1O_W3$	0.9890	0.6870	0.2880	0.104(2)	7.3(15)	4c
	$Zn1O_W4$	0.9990	0.7160	0.0930	0.104(2)	7.3(15)	4c
	$Zn1O_W5$	0.8690	0.7470	0.0890	0.104(2)	7.3(15)	4c
	$Zn1O_W6$	0.9500	0.8080	0.2200	0.104(2)	7.3(15)	4c
Zn-2	Zn2	0.7774(11)	0.1209(12)	0.8225(17)	0.071(3)	9.0 (12)	8d
OZn2	$Zn2O_W$	0.7858(12)	0.3052(17)	0.6895(21)	0.071(3)	13.6 (18)	8d
GVL	Translate	0.7641(12)	0.2334(18)	0.5610(24)			
	O1	0.7641	0.2334	0.5610	0.081(2)	8.1(32)	4c
	O2	0.8633	0.2795	0.6073	0.081(2)	8.1(32)	4c
	C1	0.8642	0.1657	0.5677	0.081(2)	8.1(32)	4c
	C2	0.9347	0.1924	0.5597	0.081(2)	8.1(32)	4c

C3	0.8230	0.2287	0.5769	0.081(2)	8.1(32)	4c
C4	0.9299	0.2580	0.6168	0.081(2)	8.1(32)	4c
C5	0.9778	0.3111	0.5788	0.081(2)	8.1(32)	4c

All the T-sites (T=Al, Si) of ZSM-5 were refined using the same B_{eq} parameter.

All the O-sites of ZSM-5 were refined using the same B_{eq} parameter.

The O-sites of Zn species were refined using the same SOF and 1.5 times of the B_{eq} for the coordinated Zn-sites.

The O-sites and C-sites of GVL were refined using the same SOF and B_{eq}.

3.4 The SXRD and Rietveld refinement of regenerated Zn/ZSM-5.

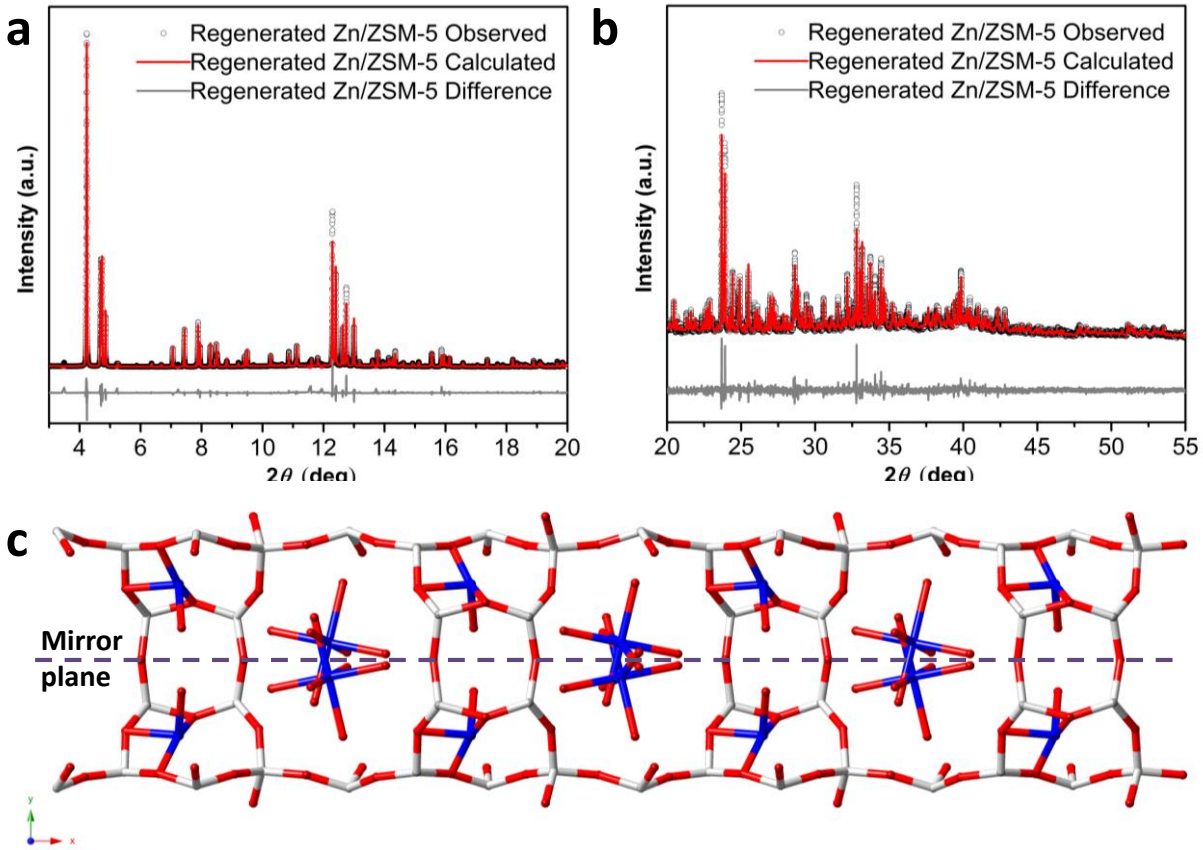

Fig. S6. SXRD with the Rietveld refinement and the structure of regenerated Zn/ZSM-5 after 310 h on-stream by air calcination, measured at room temperature. (a) Comparison of the experiment data (black circle) and Rietveld refinement (red line) and the difference between them (grey line) for SXRD patterns at a 2θ range of (a) 3 - 20° and (b) 20 - 55°. (c) The refined structure refreshed Zn/ZSM-5 (viewed from z-axis). The stick-ball model is used, with red = O, grey = Si, and blue = Zn. The symmetric Zn species between the mirror plane are illustrated (grey dotted line).

The six peaks range from 3.44-3.52°, 5.21-5.24°, 7.19-7.26°, 11.52-11.59°, 11.91-11.97° and 13.70-13.74° cannot be indexed by P*nma* and the relative intensity of these peaks were less than the 0.4% of the strongest peak, which were assumed to the impurity. These six peaks were excluded during the refinement and the R_{wp} factor decreased from 10.846% to 9.583%.

Table S5. Atomic parameters from the Rietveld refinement of regenerated Zn/ZSM-5.

Species	Atom	*x*	*y*	*Z*	SOF	B_{eq} (Å^2)	Wyckoff
Zeolite framework	O1	0.37627(47)	0.05217(67)	0.74840(62)	1	1.930(31)	8d
	O2	0.30822(53)	0.06313(45)	0.92432(62)	1	1.930(31)	8d
	O3	0.19666(50)	0.06382(42)	0.02577(47)	1	1.930(31)	8d
	O4	0.09510(40)	0.06393(54)	0.91163(70)	1	1.930(31)	8d
	O5	0.11931(49)	0.04703(64)	0.72821(65)	1	1.930(31)	8d
	O6	0.24738(47)	0.05292(68)	0.76073(64)	1	1.930(31)	8d
	O7	0.37279(49)	0.84389(51)	0.77474(72)	1	1.930(31)	8d
	O8	0.31253(52)	0.84612(40)	0.92783(63)	1	1.930(31)	8d
	O9	0.19412(55)	0.84940(32)	0.02876(51)	1	1.930(31)	8d
	O10	0.09084(47)	0.83748(47)	0.92694(79)	1	1.930(31)	8d
	O11	0.11507(48)	0.84336(52)	0.74260(73)	1	1.930(31)	8d
	O12	0.23885(49)	0.83933(53)	0.74556(72)	1	1.930(31)	8d
	O13	0.30704(50)	0.95061(50)	0.81748(49)	1	1.930(31)	8d
	O14	0.07349(40)	0.95127(59)	0.82556(59)	1	1.930(31)	8d
	O15	0.41812(48)	0.13049(51)	0.60675(79)	1	1.930(31)	8d
	O16	0.40861(51)	1.00211(51)	0.58137(76)	1	1.930(31)	8d
	O17	0.40085(54)	0.86976(47)	0.57670(82)	1	1.930(31)	8d
	O18	0.19000(60)	0.12673(46)	0.61240(64)	1	1.930(31)	8d
	O19	0.20182(60)	-0.00179(47	0.60471(65)	1	1.930(31)	8d
	O20	0.20125(60)	0.86603(44)	0.57637(66)	1	1.930(31)	8d
	O21	0.99950(51)	0.05070(64)	0.79371(61)	1	1.930(31)	8d
	O22	0.99556(53)	0.85139(55)	0.79514(64)	1	1.930(31)	8d
	O23	0.42276(71)	0.7500	0.64493(88)	1	1.930(31)	4c
	O24	0.19539(87)	0.7500	0.65962(77)	1	1.930(31)	4c
	O25	0.28321(65)	0.7500	0.05946(96)	1	1.930(31)	4c
	O26	0.10761(71)	0.7500	0.06310(08)	1	1.930(31)	4c

	Si1	0.42268(27)	0.05731(38)	0.66313(39)	1	0.957(14)	8d
	Si2	0.31141(32)	0.03239(23)	0.81680(40)	1	0.957(14)	8d
	Si3	0.27983(23)	0.05945(32)	0.03240(39)	1	0.957(14)	8d
	Si4	0.12108(25)	0.06310(32)	0.02928(40)	1	0.957(14)	8d
	Si5	0.07255(29)	0.02796(26)	0.81292(45)	1	0.957(14)	8d
	Si6	0.18820(29)	0.05554(30)	0.67390(36)	1	0.957(14)	8d
	Si7	0.42645(29)	0.83019(29)	0.67281(43)	1	0.957(14)	8d
	Si8	0.30854(32)	0.87026(26)	0.81796(37)	1	0.957(14)	8d
	Si9	0.27388(27)	0.82846(26)	0.03130(44)	1	0.957(14)	8d
	Si10	0.11955(30)	0.82418(28)	0.03265(46)	1	0.957(14)	8d
	Si11	0.07269(28)	0.87268(30)	0.82042(44)	1	0.957(14)	8d
	Si12	0.18853(35)	0.82559(24)	0.68567(41)	1	0.957(14)	8d
Zinc 1	Translate	0.9623(11)	0.7203(17)	0.2110(15)			
	Zn1	0.9624	0.7203	0.2110	0.126(2)	10.2(13)	4c
	$Zn1O_W1$	0.9380	0.6172	0.1970	0.126(2)	15.3(19)	4c
	$Zn1O_W2$	0.8647	0.7400	0.2620	0.126(2)	15.3(19)	4c
	$Zn1O_W3$	0.9930	0.7030	0.3601	0.126(2)	15.3(19)	4c
	$Zn1O_W4$	1.0600	0.7000	0.1600	0.126(2)	15.3(19)	4c
	$Zn1O_W5$	0.9310	0.7370	0.0620	0.126(2)	15.3(19)	4c
	$Zn1O_W6$	0.9870	0.8233	0.2260	0.126(2)	15.3(19)	4c
Zinc 2	Zn2	0.7802(16)	0.1197(15)	0.8209(24)	0.061(1)	12.2(20)	8d
O2	$Zn2O_W1$	0.7858(12)	0.3052(17)	0.6895(21)	0.061(1)	18.4 (30)	8d

All the T-sites (T=Al, Si) of ZSM-5 were refined using the same B_{eq} value.

All the O-sites of ZSM-5 were refined using the same B_{eq} value.

The O-sites of hexa-aqua Zn-1 complex were refined using the same SOF and 1.5 times of the B_{eq} .

4 EXAFS

Local structures surrounding the Zn atoms were probed by using extended x-ray absorption fine structure (EXAFS) technique on beamline BL07A of Taiwan Light Source at National Synchrotron Radiation Research Center (NSRRC) in Taiwan. A Si(111) double crystal monochromator was used to scan the photon energy. The energy resolution ($\Delta E/E$) for the incident X-ray photons was estimated to be 2×10^{-4}. The conventional transmission mode was adopted for Zn K-edge EXAFS measurements. To ascertain the reproducibility of the experimental data, at least two scan sets were collected and compared for each sample. The EXAFS data analysis was performed using IFEFFIT 1 with Horae packages 2 (Athena and Artemes). The spectra were calibrated with foils as a reference. And the amplitude parameter was obtained from EXAFS data analysis of the Zn foil, which was used as a fixed input parameter in the data fitting to allow the refinement in the coordination number of the absorption element. In this work, the first shell data analyses under the assumption of single scattering were performed with the errors estimated by R-factor.

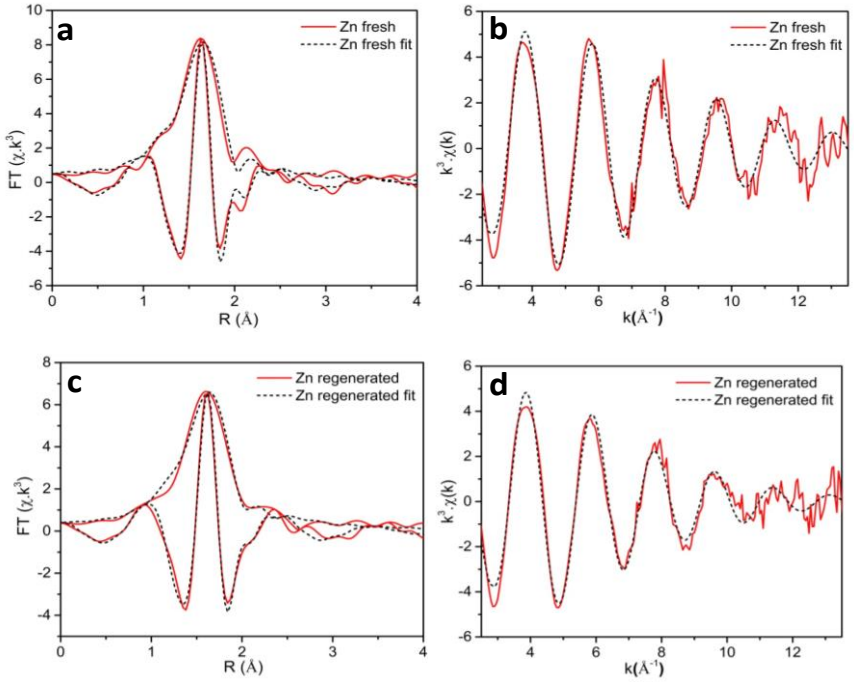

Fig. S7. EXAFS data and the best fitted Zn/ZSM-5. (a) The K^3-weighted Fourier transformed EXAFS at the Zn K-edge of (a) fresh Zn/ZSM-5, (b) regenerated Zn/ZSM-5, and the corresponding K^3-weighted experimental and the simulated data (c) and (d). The measured spectra are plotted in red, and the simulated spectra are plotted in black.

Table S6. Summary of the refinement results of GVL adsorbed on fresh Zn/ZSM-5 and regenerated Zn/ZSM-5.

Sample	Zn-1 species	(Å)	Zn-2 species	(Å)	GVL	(Å)
Fresh sample	Zn-1 – O(H_2)	2.12(3)	Zn-2 – O6	1.92(2)	C_{GVL} - Zn-2–O(H)	1.82(4)
			Zn-2 – O9	2.19(3)	O_{GVL} – O6	3.34(8)
			Zn-2 – O18	1.95(2)		
			Zn-2 – O(H)	2.32(5)		
Regenerated sample	Zn-1 – O(H_2)	2.12(3)	Zn-2 – O6	1.85(2)		
			Zn-2 – O9	2.17(2)		
			Zn-2 – O18	2.03(2)		
			Zn-2 –O(H)	2.31(2)		

The errors of distances were calculated from the percent errors of the translational (x, y, z) multiply by distances.

5 Isotope labelling experiment with water-^{18}O ($H_2{}^{18}O$)

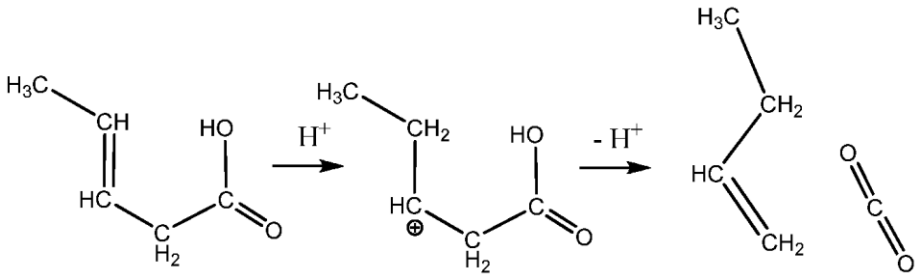

Scheme S1. Brønsted acid catalysed conversion of GVL to 1-butene and CO_2

Brønsted Acid site can catalyse ring opening of GVL to form 1-butene and CO_2 as shown in the above mechanism in Scheme S1[5].

To differentiate this reported acid site catalysed ring opening mechanism from our proposed mechanism induced by Zn-OH (Scheme S2), isotope labelling experiment was conducted. The 40 wt% GVL substrate was mixed with $H_2{}^{16}O$ or $H_2{}^{18}O$. The gas phase products of the GVL conversion in the presence of $H_2{}^{18}O$ and nitrogen were monitored by GC-MS. The gas was first collected from the outlet of the reactor at room temperature for 0.5 h before it was injected for GC-MS measurement.

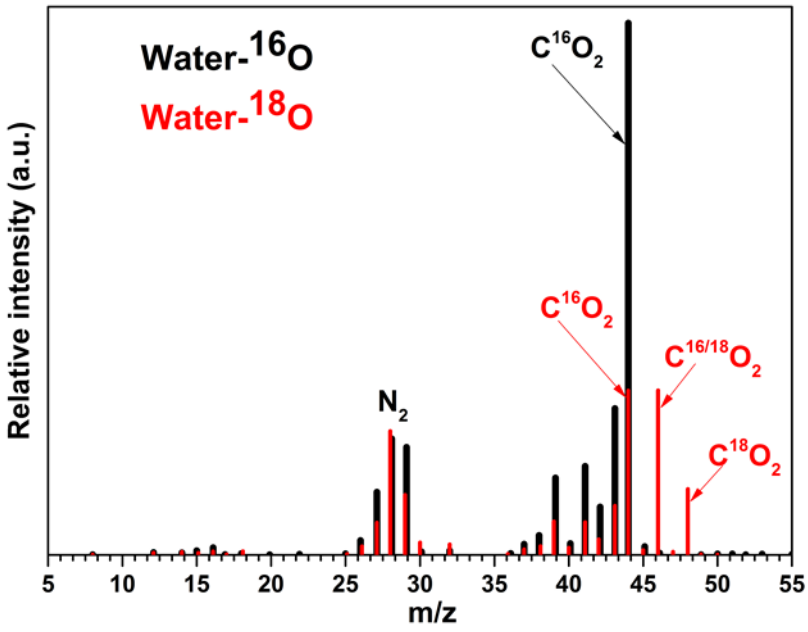

Fig. S8. Mass spectrum of the gas phase products of the GVL aromatization experiment in the presence of water-^{18}O ($H_2{}^{18}O$) or water-^{16}O ($H_2{}^{16}O$) (residual time: 1.028 min).

The main peak at 44, 46 and 48 m/z can be assigned to $C^{16}O_2$ (also contained propane), $C^{16/18}O_2$ and $C^{18}O_2$, respectively. After switching to $H_2{}^{18}O$ (99% enriched from Sigma Aldrich), the peak at 44 m/z ($C^{16}O_2$) which was originally the highest peak in the presence of water-^{16}O, substantially

decreased with the formation of new peaks at 46 ($C^{16/18}O_2$) and 48 m/z ($C^{18}O_2$). As seen from Fig. S8, the ratios of these three peaks are found to be $C^{16}O_2$: $C^{16/18}O_2$: $C^{18}O_2$ = 2 : 2 : 1. Despite a small degree of scrambling between labelled oxygen from heavy water and GVL[6] as well as $H_2{}^{18}O$ and $C^{16}O_2$ in gas phase (no H_2 was detected) there is a clear large enrichment of $C^{16/18}O_2$. This indicates that the proposed mechanism for ring opening of GVL to form 1-butene and CO_2 over solid acid site by Dumesic and co-workers as shown in the above mechanism in Scheme S1[7] is not the dominant process (account only for $C^{16}O_2$). Instead, the labelling water-^{18}O must have been also involved in the catalysis for the water induced hydrolysis of GVL to 1-butene and CO_2 (account for $C^{16/18}O_2$). The small quantity of $C^{18}O_2$ might have produced from steam reforming of 'carbon' deposit by water-^{18}O during the catalysis.

6 Solid state NMR

All NMR experiments were performed on 400WB AVANCE III spectrometer at room temperature. The various protons of solid state catalysts (Zn/ZSM-5) were first characterized through ^{1}H MAS NMR, based on their chemical shift values. Before the ^{1}H MAS NMR measurement, the sample was introduced into a glass tube, which was then connected to a vacuum system. The pretreatment was carried out at 300 °C for 8 h under vacuum (10^{-1} Pa) and cooled down to the room temperature. Then the content of the glass tube was transferred to a glove box. Under dry nitrogen, the sample was packed into a 1.9 mm ZrO_2 rotor and sealed with Kel-F lids. ^{1}H MAS NMR spectra were acquired at resonance frequency of 400.4 MHz, using 90° pulses with a recycle delay of 5 s at a MAS speed of 15.0 kHz. Tetramethylsilane was used as a standard sample for chemical shift reference and the external intensity standard to quantify the signal in ^{1}H MAS NMR spectra.

For the ^{31}P MAS NMR measurement, the sample was introduced into a glass tube, which was then connected to a vacuum system. The pretreatment was carried out at 573 K for 2 h under vacuum (10-1 Pa). After adsorption of gaseous trimethylphosphine (TMP) at room temperature at steady conditions, the glass tube was then isolated and immersed in liquid nitrogen. Then the content of the glass tube was transferred to a glove box. Under dry nitrogen, the sample was packed into a 4 mm ZrO2 rotor and closed with Kel-F lids. All NMR experiments were performed on 400WB AVANCE III spectrometer at room temperature. ^{31}P high powered decoupling (HPEDC) MAS NMR spectra were acquired at resonance frequency of 161.9 MHz, using 30° pulses with a recycle delay of 15 s at a MAS speed of 12 kHz. $NH_4H_2PO_4$ was used as a standard sample for chemical shift reference of P. Thus, the external intensity standards were used to quantify the signals in ^{1}H MAS NMR and ^{31}P MAS NMR spectra. The fresh and regenerated Zn/ZSM-5 samples were found to be identical through ^{1}H MAS NMR and ^{31}P MAS NMR spectroscopy, based on the chemical shift values. Typically, the peak at -5 ppm corresponds to the interaction between TMP and the Brønsted acid site introduced by Zn-OH (Fig. S9). Another asymmetric peak with lower intensity around -61 ppm corresponds to weak interaction between TMP and the Lewis acid sites of the non-framework aluminum.

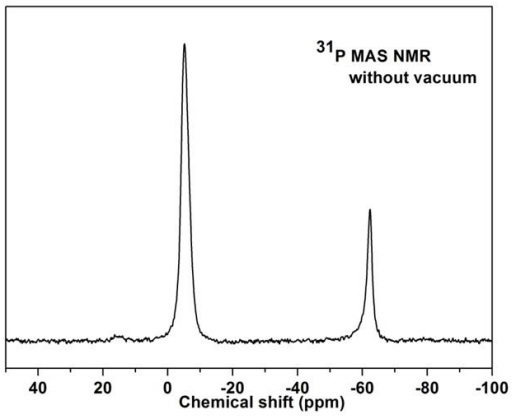

Fig. S9. Solid state ^{31}P MAS NMR spectrum of adsorbed TMP on Zn-ZSM-5 without vacuum.

From the difference in electron density, we should be able to differentiate between six (the formation of dealuminated species during to the hydrolysis at high temperature to account for deactivation) from normal four coordinate. Al^{27}Al MAS NMR was used to detect the coordination of Al in H-ZSM-5. The ^{27}Al MAS NMR spectrum was obtained using 400WB AVANCE III, at the Larmor frequency of 104.34 MHz. The one pulse sequence was adopted, with a 10° pulse, a delay time of 0.4 s and a scanning number of 8000. The chemical shift was referenced to 1 M $AlCl_3$ aqueous solution.

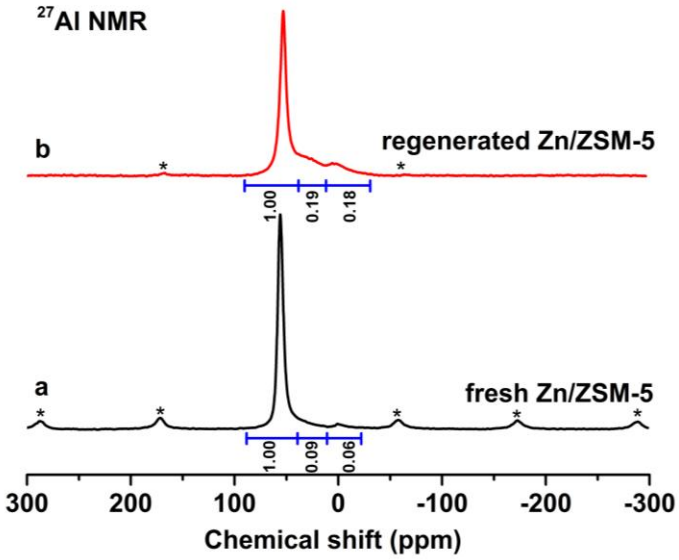

Fig. S10. Solid-state ^{27}Al MAS NMR spectra of (a) fresh Zn/ZSM-5 and (b) regenerated Zn/ZSM-5 after 310 h on-stream by air calcination. The asterisk denotes a spinning sideband.

In ^{27}Al MAS NMR spectrum (Fig. S10), the chemical shifts at *ca*. 1 and 55 ppm correspond to the six-coordinate extra-framework Al species and the four-coordinate framework Al species

respectively. The broad peak between 1 ppm and 55 ppm is attributed to the five-coordinate Al species. In the fresh and regenerated Zn/ZSM-5 catalysts, the intensity and area of the peak at *ca*. 55 ppm is significantly larger than the peak at *ca*. 1 ppm, which reflects the dominance of the framework Al species. By integrating the peak areas, the ratio of the four-coordinate framework Al, the five-coordinate Al and the six-coordinate extra-framework Al in the fresh and regenerated Zn/ZSM-5 after Cycle III is 87%/8%/5% and 73%/14%/13%, respectively. The slight difference indicates most of the aluminium still remained in the framework after 310 h of reaction. Anestimation for a maximum of 14% framework aluminium could be hydrolyzed to extra-framework aluminium. This suggests that the two structures are almost identical to each other.

7 Total Catalyst Regeneration

The Zn/ZSM-5 catalyst is as a typical microporous acidic zeolite. We have found that it was gradually deactivated during 310 h of on-stream testing. However, the deactivated Zn/ZSM-5 catalyst can be regenerated to the same catalytic activity through air calcination at 600 ℃ for 1 h. The total value of 0.99 Zn by adding SOFs of Zn-1 and Zn-2 is also obtained from the regenerated sample (Table S5). Similarly, the derived coordination numbers and corresponding Zn-O distances from EXAFS and SXRD refinement (Table 1 and Table S6) of the regenerated sample also clearly indicate the structural integrity of the active site in Zn/ZSM-5 after the prolonged testing.

8 New Cooperative ring-opening decarboxylation route

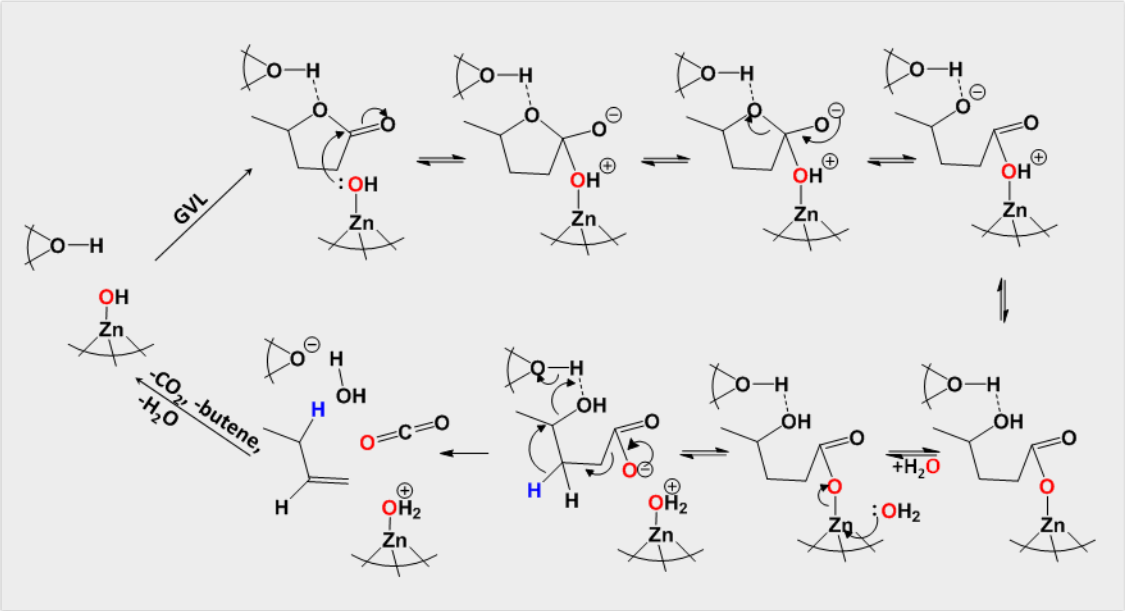

Scheme S2. The proposed mechanism for aromatics production from cooperative ring opening hydrolytic decarboxylation of gamma-valerolactone (GVL) with water molecule activation over Zn/ZSM-5.

The proposed mechanism for aromatics production from cooperative ring opening hydrolytic decarboxylation of gamma-valerolactone (GVL) with water molecule activation over Zn/ZSM-5 by the regenerative Zn-OH and Brønsted acid site to CO_2 and 1-butene where the latter can further undergo aromatization in the ZSM-5 cage. This route is different from the Brønsted Acid catalysed conversion of GVL to 1-butene and CO_2 as described in Scheme S1.

9 Spectroscopic characterization of Zn/ZSM-5

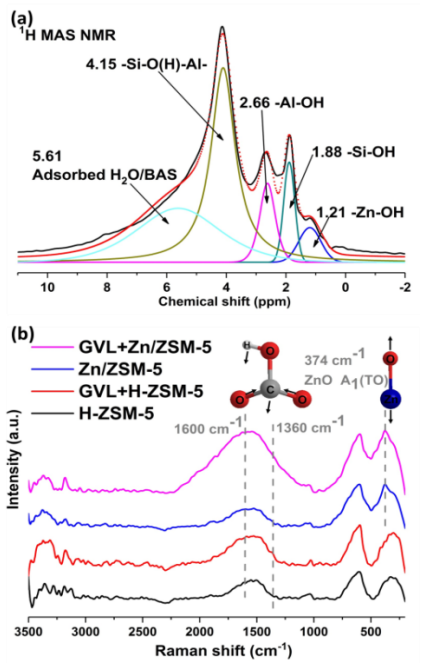

Fig. S11. (a). ^{1}H MAS NMR of fresh Zn/ZSM-5 at 30 ^{o}C, after vacuum pre-treatment at 300 ^{o}C for 8 h, experimental data (black line), simulated data (red dot) and the corresponding simulated partial contributions (blue, green, violet, dark yellow and light blue line). (b) Raman spectra of various samples. They show clearly a characteristic large peak and wide broadening of Raman absorption frequencies near 1100-2240 cm^{-1} which encompasses -C=O of GVL at ca. 1600 cm^{-1} and symmetrical O-C-O at 1360 cm^{-1} upon the GVL adsorption on Zn/ZSM-5. In addition, the A1 (TO) mode of Zn-O at 374 cm^{-1} is visible on the terminal Zn-OH in Zn/ZSM-5.

Raman spectroscopy was employed to study the adsorbed structure of GVL on Zn/ZSM-5, see Fig S11 (also Fig. 3b in main text). The spectrum shows clearly a much larger and broader peak with Raman frequencies near the 1100-2240 cm^{-1} region. The formation of this peak upon the GVL adsorption on Zn/ZSM-5 encompasses -C=O of GVL at *ca.* 1600 cm^{-1} and symmetrical O-C-O at 1360 cm^{-1} and various modes of HCO_3^- [8]. In addition, the A_1(TO) mode of Zn-O at 374 cm^{-1} is also observed upon the adsorption of GVL on the terminal Zn-OH in Zn/ZSM-5. According to the pervious report, the A_1(TO) mode of pure Zn-O (vibration mode inserts) exhibits a band at 382 cm^{-1}. However, the hetero-structure of Zn-O and the supported Zn-O A_1(TO) modes are expected to be significantly weaker than that of pure Zn-O, and the A_1(TO) can also be red-shifted by 10 cm^{-1} due to the support effect[9]. Hence, the Raman frequency at 374 cm^{-1} is attributed to the supported Zn-O.

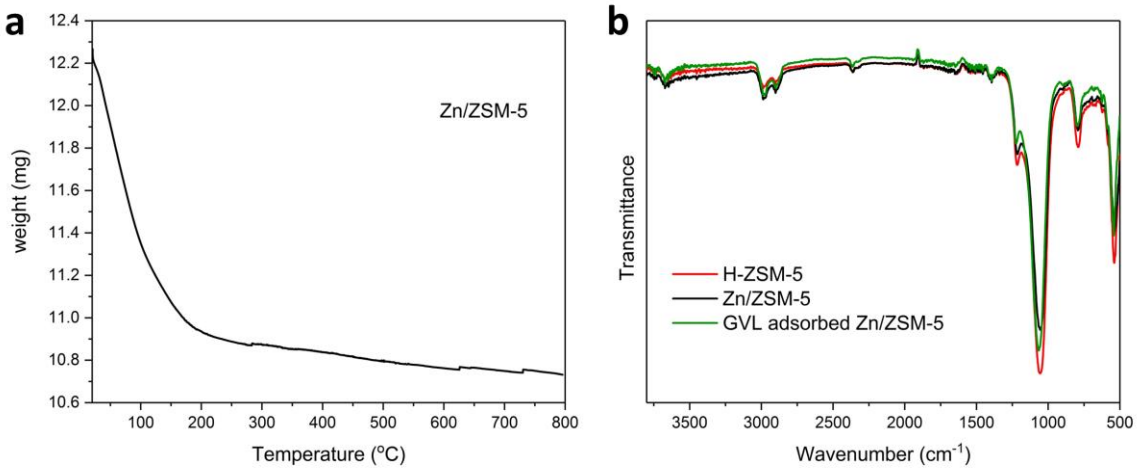

Fig. S12. (a) The thermogravimetric (TG) analysis of fresh Zn/ZSM-5, and (b) FT-IR spectra of H-ZSM-5, Zn/ZSM-5 and GVL adsorbed Zn/ZSM-5.

As seen from Fig. S12a, we studied the weight loss of the Zn/ZSM-5 sample by the thermogravimetric (TG) analysis. The weight loss is primarily caused by the elimination of water molecules from the structure. A majority of physisorbed water and water from surface dihydroxylation are taken place at below 550°C (Journal of Molecular Catalysis A: Chemical 139 1999 199–207). However, from 550 to 800 °C (above the calcination temperature), the weight lost continues to take place until 800 °C (cumulative to 0.08 mg) which is equivalent to 2.6 H_2O per unit cell. This matches with the expected number of the stable coordinated water in hexa-aqua Zn-1 per unit cell. Note that, as mentioned in the main text, there are 0.42 hexa-aqua Zn-1, hence corresponding to 2.52 of the ligand H_2O per unit cell. We acknowledge that a part of the weight loss of 0.08 mg from 550 to 800 °C may be caused by the dehydration of isolated Si or Al terminal -OH groups, but their contributions are believed to be minimal. Therefore, by combining the evidence of SXRD, structural refinement, EXAFS and TG, Zn-1 is still in the form of hexa-aqua Zn^{2+} after the sample pre-treatment. The FT-IR (Fourier transformed-infrared) spectra of H-ZSM-5, Zn/ZSM-5 and GVL adsorbed Zn/ZSM-5 are shown in Fig. S12b. They give typical symmetric and non-symmetric Si-O vibration frequencies from 500 to 4200 cm^{-1}[10]. The stretching mode of water *ca*. 3600 to 3750 cm^{-1} indicates the presence of structural OH group, which overlaps with the characteristic absorption band at 3654 cm^{-1} of the Zn–OH group (reference 18 in the main text). The band at 1049 and 1211 cm^{-1} are assigned to the asymmetric stretching of Si-O and Al-O bonds. The band at 789 cm^{-1} is assigned to Si-O symmetric stretching mode. The band at 539 cm^{-1} arises from structural double D5R rings of MFI structure[10].

The hexa-aqua Zn-1 in the cross-channel region of Zn/ZSM-5 is likely maintained by the surrounding negatively charged framework oxygen atoms through electrostatic interaction by ion-exchange with the Brønsted acid sites. According to our modelling as shown in Fig. S13, the Zn-1

specie may partial block one of the sinusoidal channels. However, it is not bulky enough to lead to a complete blockage of the adjacent straight channel. Hence, reaction gases can still pass through to this straight channel. In addition, the concentration of Zn-1 is relatively low (0.42 Zn-1 versus 4 asymmetric units per unit cell). Thus, severe physical blocking by Zn-1 affecting the reaction is not significant.

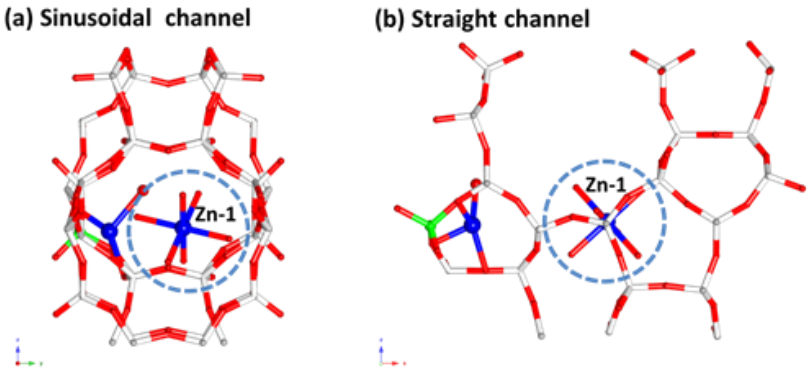

Fig. S13. The crystal structure viewing from the (a) sinusoidal (x-axis) and (b) straight (y-axis) channel.

10 Remarks in Mechanism

As pointed out in the introduction, extensive structural studies of Zn inclusions in various zeolites have previously been described by experimental and theoretical works in a number of publications (i.e Microporous Mesoporous Mater. 1998, 24, 101-112., J. Am. Chem. Soc. 2013, 135, 13567-13573., J. Mol. Catal. A: Chem. 2005, 237, 36-44 and Kinet. Catal. 2013, 54, 744-748, etc). However, our present SXRD, refinement and associated analysis not only reveal the immobilised Zn structures in ZSM-5 but also the unique surface adduct with GVL in 3-D manner.

From the synchrotron X-ray powder diffraction (SXRD), we have disclosed two isolated Zn species from the extra electron-rich regions within the zeolite cavity. By combining with the EXAFS experiments, a hexa-aqua Zn^{2+} (labelled as Zn-1) is found at the intersection region of the sinusoidal and straight channels, whereas a tetrahedrally coordinated Zn^{2+} (labelled as Zn-2) containing terminal Zn-OH is anchored onto the framework oxygen atoms next to Al(T6) of ZSM-5. By considering the symmetry of Zn/ZSM-5 and the site occupancy factors (SOF) derived from SXRD, there are 0.42 Zn-1 and 0.57 Zn-2 per unit cell. It is also found that the carbonyl of GVL molecule only aligns itself towards the terminal Zn-OH of the Zn-2 at RT, suggesting the tendency for further catalysis reaction at high temperature (nucleophilic attack of GVL by Zn-OH). From the ^{1}H MAS NMR experiment and Raman spectroscopy, the terminal Zn-OH of the Zn-2 can also be identified, see Section S9. In short conclusion here, the ^{1}H MAS NMR and Raman spectroscopy experiments have clearly demonstrated the existence of the Zn-OH group and corresponding vibrations of Zn-O in this catalyst. We have argued that this immobilised Zn-2 with the terminal Zn-OH plays a contributing factor for the rate enhancement in GVL conversion due to its strong nucleophilic nature towards GVL. Thus, the additional Zn^{2+} by ion exchange into H-ZSM-5 clearly promotes its activity and catalytic lifetime.

The labelling experiment using water-^{18}O suggested that water must have also been involved in the catalysis for the water induced hydrolysis of GVL to 1-butene and CO_2 (Fig. S8).

It is noted that we cannot exclude the possibility of GVL that may also interact with Zn-1 (presumably via one of its coordinated saturated H_2O ligand) and contribute to the overall catalytic activity. It is because our approach cannot apply to those GVL-Zn-1 species if they are non-crystallized and hence cannot rule out their existence. Despite the polarisation by Zn^{2+} it is however envisaged that the non-dissociated H_2O molecule cannot act as a strong nucleophile as that of Zn^{2+}-OH^- for the rapid GVL attack. Similarly, without the presence of Zn^{2+}, the BAS sites are also unable to polarize a water molecule to asymmetric OH^- and H^+.

In addition, the favourable dissociative adsorption of water molecule on immobilised Zn^{2+} and $(Si\text{-}O\text{-}Al)^-$ in H-ZSM-5 to form $(Zn\text{-}OH)^+$ and (Si-O(H)-Al) has been demonstrated by both FTIR (the appearance of a new absorption band at 3654 cm^{-1} due to the formation of Zn–OH groups at 573K) and DFT calculations (The DFT cluster calculations for the dissociative H_2O adsorption on Zn^{2+} stabilized in zeolite cation positions at a close proximity with the sufficient spatial separation of two lattice Al atoms render the energetics favourable) in the literature (reference 18 in the main text). This study matches well with our above observations. That means water molecule can be used as substrate to regenerate the immobilised Zn-2 with terminal Zn-OH dissociatively at high temperature (in a close proximity of BA) after its consumption in the nucleophilic reaction. More importantly, the nucleophilicity of M-OH in our study of dopers also follows the same order for their catalytic activity: Zn > Ga > Sn. This trend can be rationalised by the order of electronegativity: Zn(1.65) < Ga(1.81) < Sn(1.96). Hence, the electron density of the 'O' of the M-OH group follows the trend: Zn-OH > Ga-OH > Sn-OH.
It is noted that the Zn-containing enzymes also regenerates its terminal OH from dissociative water activation via its deprotonated site for a similar nucleophilic attack.
Thus, we believe that this new regenerable Zn-OH route in water at high temperature in Zn/ZSM-5 can clearly play a significant part to contribute to the enhanced GVL conversion rate.

The net charges of these species and their interactions with the zeolite framework are shown as follows:

(1) For every Zn^{2+} immobilised, two equivalent BAS(H^+) as $[Al\text{-}O\text{-}Si]^-H^+$ of H-ZSM-5 in close proximity will be chemically exchanged.
(2) After calcination, 0.42 per unit cell of hexa-aqua Zn-1 as $Zn(H_2O)_6^{2+}$ is found remaining in the porous cavity of Zn/ZSM-5 while 0.57 per unit cell of tetrahedral Zn-2 stabilised by the deprotonated BAS $[Al\text{-}O\text{-}Si]^-$ wall of ZSM-5 with a terminal Zn-OH.
(3) The stoichiometric equation and charge balance for the dissociative water molecule regeneration of immobilized Zn^{2+} after the -OH consumption for its nucleophilic reaction is shown as follows:
$[Al\text{-}O\text{-}Si]^-\text{–}Zn^{2+} + [Al\text{-}O\text{-}Si]^- + H_2O \rightarrow [Al\text{-}O\text{-}Si]^- - [Zn^{2+}\text{–}OH^-]^+ + [Al\text{-}O\text{-}Si]^-H^+$

where the tetrahedrally coordinated Zn-2 species is anchored on the framework, which means the Zn(II) is simultaneously stabilised by three framework oxygen atoms (O6, O9, O18).

References:

[1] S. P. Thompson, J. E. Parker, J. Potter, T. P. Hill, A. Birt, T. M. Cobb, F. Yuan, C. C. Tang, *Rev. Sci. Instrum.* **2009**, *80*.

[2] N. H. Heo, C. W. Kim, H. J. Kwon, G. H. Kim, S. H. Kim, S. B. Hong, K. Seff, *J. Phys. Chem. C* **2009**, *113*, 19937-19956.

[3] P. Thompson, D. E. Cox, J. B. Hastings, *J. Appl. Crystallogr.* **1987**, *20*, 79-83.

[4] Y. F. Xue, A. Liljas, B. H. Jonsson, S. Lindskog, *Proteins: Struct., Funct., Genet.* **1993**, *17*, 93-106.

[5] J. Q. Bond, D. M. Alonso, D. Wang, R. M. West, J. A. Dumesic, *Science* **2010**, *327*, 1110-1114.

[6] G. Liu, D. Willcox, M. Garland, H. H. Kung, *J. Catal.* **1985**, *96*, 251-260.

[7] Y. Y. Chu, Z. W. Yu, A. M. Zheng, H. J. Fang, H. L. Zhang, S. J. Huang, S. B. Liu, F. Deng, *J. Phys. Chem. C* **2011**, *115*, 7660-7667.

[8] E. Garand, T. Wende, D. J. Goebbert, R. Bergmann, G. Meijer, D. M. Neumark, K. R. Asmis, *J. Am. Chem. Soc.* **2010**, *132*, 849-856.

[9] Y. Dong, C. Feng, P. Jiang, G. Wang, K. Li, H. Miao, *Rsc Adv.* **2014**, *4*, 7340-7346.

[10] P. Morales-Pacheco, J. M. Dominguez, L. Bucio, F. Alvarez, U. Sedran, M. Falco, *Catal. Today* **2011**, *166*, 25-38.